




Effects of Chromatic Dispersion on Single-Photon Temporal Wave Functions in Quantum Communications

Artur Czerwinski ^{1,*}, Xiangji Cai ^{2,†} and Saeed Haddadi ^{3,‡}

¹*Centre for Quantum Optical Technologies, Centre of New Technologies, University of Warsaw, Banacha 2c, 02-097 Warszawa, Poland*

²*School of Science, Shandong Jianzhu University, Jinan 250101, China*

³*Faculty of Physics, Semnan University, P.O. Box 35195-363, Semnan, Iran*

In this paper, we investigate the effects of chromatic dispersion on the temporal wave functions (TWFs) of single photons in the context of quantum communications. We start by considering TWFs defined by generalized Gaussian modes. From this framework, we derive two specific models: chirped and unchirped Gaussian TWFs. In the first case, we explore the impact of the chirp parameter on the properties of single-photon TWFs. We show that by properly adjusting the chirp parameter, it is possible to compensate for the detrimental effects of chromatic dispersion, allowing for the maintenance of high-fidelity transmission of quantum information over long distances. Furthermore, we examine the effects of chromatic dispersion on a qubit defined in the time domain, illustrating how this phenomenon can influence the transmission of information encoded in time-bins. Finally, we consider non-Gaussian TWFs that are represented by hyperbolic-secant modes. Our results provide important insights into the design and implementation of high-speed and long-distance quantum communication systems. The findings underscore the potential for using chirp management techniques to mitigate the effects of chromatic dispersion.

Keywords: Chromatic dispersion; Single photons; Gaussian modes; Chirp parameter; Single-photon temporal wave function; Time-bin qubits

I. INTRODUCTION

Quantum communications is a branch of quantum mechanics that deals with the transmission and manipulation of quantum states of light or matter to facilitate the exchange of information [1, 2]. It is an area of active research, with the goal of developing secure, high-speed, and long-distance communication systems based on quantum mechanical principles [3–5].

In practice, Gaussian pulses are often used as a model for optical pulses generated by laser sources, as they closely approximate the shape of the pulses generated in these systems [6]. Gaussian pulses are used in a variety of quantum communication protocols, such as continuous-variable quantum key distribution (CV-QKD), quantum teleportation and time-bin encoding [7–9]. In CV-QKD, Gaussian pulses are used to encode the quantum state of a light field, which can then be transmitted over an optical fiber to a remote receiver. The receiver measures the light field and uses the information contained in the Gaussian pulse to establish a shared secret key with the sender [10, 11]. In quantum teleportation, Gaussian pulses are used to transfer the quantum state of a light field from one location to another. This is done by first entangling a pair of light fields, and then transmitting one of the light fields (the “idler”) to the receiver. The sender then encodes the quantum state of the light field to be teleported onto the other light field (the “signal”),

and sends it to the receiver. The receiver then uses the entanglement to reconstruct the original quantum state of the light field [12, 13]. In both of these protocols, the shape and quality of the Gaussian pulses are critical for achieving high-fidelity transmission of the quantum information. Therefore, techniques such as chirp management and dispersion compensation are often used to preserve the shape of the Gaussian pulses over long distances.

In time-bin encoding, Gaussian wave packets are used to represent the quantum state of a single photon in the time domain, rather than the traditional frequency or spatial domains [14–16]. Exploiting the time-bin degree of freedom allows for encoding quantum information in terms of the relative arrival times of photons. This technique offers a particularly robust type of quantum information [17]. Advantages of time-bin encoding were demonstrated in 1999 by the Group of Applied Physics from the University of Geneva [18]. They generated arbitrary time-bin qubits by sending a single-photon wave packet through a Mach–Zehnder interferometer. Due to a difference in the length of the optical paths, the photon wave packet leaves the interferometer in a quantum-mechanical superposition of “early” and “later” time bins. The Geneva team became renowned for demonstrating the ability of time-bin qubits to travel extended distances through optical fibers with minimal decoherence.

In quantum communications, the light pulse can be affected by a variety of factors that can degrade the quality of the quantum state being transmitted, including chromatic dispersion, noise, photon loss, and misalignment [19]. Chromatic dispersion is a phenomenon that occurs in optical fibers, where different wavelengths of light travel at slightly different speeds [20]. This results in a

* aczerwin@umk.pl

† xiangjicai@foxmail.com

‡ haddadi@semnan.ac.ir

spreading out of a pulse of light as it propagates through the fiber, which can cause distortion and limit the maximum distance that a signal can travel [21, 22]. Chromatic dispersion depends on a variety of factors, including the properties of the fiber itself and the way that the fiber is manufactured. In general, the destructive effects of chromatic dispersion can be mitigated by using dispersion-compensating fibers or devices [23–25]. However, under some circumstances, the distance of secure communication can be extended by introducing additional dispersion [26].

The second-order dispersion parameter, also known as the group velocity dispersion (GVD) parameter, is a measure of the variation of the group velocity of light with wavelength in an optical fiber. It is typically specified in units of ps^2/km and is used to predict the amount of pulse spreading that will occur in a fiber over a given distance. Positive GVD indicates normal dispersion, where longer wavelengths travel slower than shorter wavelengths, and negative GVD indicates anomalous dispersion, where longer wavelengths travel faster than shorter wavelengths. The GVD parameter is important in the design of high-speed optical communication systems, as it determines the maximum bit rate that can be transmitted over a given length of fiber.

Chromatic dispersion, an intrinsic phenomenon in optical systems, leads to the temporal spreading of light pulses, which is a well-studied topic in classical optics [27, 28]. However, our study takes a pioneering approach by delving into the realm of quantum mechanics, focusing on the characteristics of single-photon temporal wave functions (TWFs) [29] instead of classical pulses of light. This novel perspective is essential because quantum technologies, such as quantum key distribution and quantum teleportation, often rely on precise control and manipulation of single-photon states. By investigating how chromatic dispersion affects the temporal modes of single photons, this paper not only enhances our fundamental understanding of the quantum behavior of light but also provides valuable insights for the development of quantum optical systems that can mitigate dispersion-induced limitations, thereby pushing the boundaries of quantum information science and technology.

The paper is organized as follows. Sec. II contains preliminaries related to theoretical background and notations. In Sec. III, we discuss the broadening of single-photon TWFs represented by generalized Gaussian modes. Based on such a general type of the temporal mode, two specific cases can be distinguished. First, Sec. IV covers an examination of the effects of chromatic dispersion on Gaussian modes, involving the impact of the chirp parameter. Second, in Sec. V, we present an analysis of the impact of chromatic dispersion on unchirped Gaussian modes. Moreover, Gaussian modes can be applied to define a time-bin qubit and investigate its properties under chromatic dispersion, which is demonstrated in Sec. VI. We extend the scope of the paper beyond the Gaussian-shaped TWFs by cover-

ing hyperbolic-secant modes in Sec. VII. Finally, in Sec. VIII, we present the summary of findings, conclusions, and future research suggestions.

II. THEORETICAL PRELIMINARIES

A single-photon TFW provides a mathematical description of the state of a photon with respect to time. It is a complex-valued function that indicates the probability amplitude of finding the photon at a particular moment in time. Throughout the paper, this object shall be denoted by $\psi(t)$.

The square of the magnitude of the wave function gives the probability density function (PDF) of the existence of the photon at a specific temporal point, i.e. $|\psi(t)|^2 = \psi^*(t)\psi(t) \equiv p(t)$. We consider only the normalized TWFs, which means that $\int_{-\infty}^{\infty} \psi^*(t)\psi(t) dt = 1$. The width of a TWF can be characterized by the standard deviation (SD), denoted by σ and obtained as the square root of the variance. We will compute

$$\sigma = \sqrt{\int_{-\infty}^{\infty} t^2 p(t) dt}, \quad (1)$$

assuming that the PDF is a zero-mean distribution, i.e. $\int_{-\infty}^{\infty} t p(t) dt = 0$.

Then, we investigate how the TFW changes as a photon propagates through a dispersive medium, like a fiber or the air in the case of free-space optics (FSO). To mathematically represent the effects of chromatic dispersion, we implement a propagator, $\mathcal{S}(t, \tau, L)$ [30–32], which acts on the initial TWF as

$$\psi_L(t) := \int_{-\infty}^{\infty} \mathcal{S}(t, \tau, L) \psi(\tau) d\tau. \quad (2)$$

The propagator $\mathcal{S}(t, \tau, L)$ can be represented as

$$\mathcal{S}(t, \tau, L) = \frac{1}{2\sqrt{\pi i \beta L}} \exp\left(\frac{i(t - \tau)^2}{4\beta L}\right), \quad (3)$$

where L denotes the propagation distance and β stands for the second-order dispersion parameter of the medium, i.e. the GVD parameter.

For the TFW affected by the propagator, we can compute the PDF, which is denoted by $p_L(t)$. Then, we proceed analogously as in Eq. (1) to calculate the width of the distribution after the transmission of the signal (σ_L). Finally, to quantify the effects of chromatic dispersion, we introduce the broadening parameter defined as

$$\Gamma = \frac{\sigma_L}{\sigma}, \quad (4)$$

which can indicate that the TFW has become either wider (for $\Gamma > 1$) or narrower (for $\Gamma < 1$) than the initial one.

Another figure of merit is introduced in the context of quantum communications. If we assume that every photon carries quantum information encoded, for example, in

the photon's polarization, we must determine a detection window related to the symbol duration time. Here, we follow the so-called three-sigma rule, which claims that nearly all values of a random variable lie within three SDs of the mean. Then, the symbol duration time after propagation through a dispersive medium can be defined as $\mathcal{T}_S := 6\sigma_L$. The symbol duration time allows one to compute the symbol rate as $f_S := (\mathcal{T}_S)^{-1}$. The symbol rate is measured in baud (Bd) meaning symbols per second. This figure provides an upper boundary of the attainable gross bit rate in quantum communications with single photons.

III. BROADENING OF GENERALIZED GAUSSIAN MODES

A. Methods

Let us start with a framework for photons characterized by generalized Gaussian temporal modes. In this case, we use the properties of generalized Gaussian distribution (GGD) and represent the TWF as

$$\psi(t) = \sqrt{\frac{q}{2\alpha\Gamma(1/q)}} \exp\left(-\frac{1+iC}{2\alpha^q}|t|^q\right), \quad (5)$$

where $\alpha = \sigma\sqrt{\Gamma(1/q)/\Gamma(3/q)}$ with the Gamma function $\Gamma(s) = \int_0^\infty x^{s-1}e^{-x}dx$ ($s > 0$), σ representing the SD of PDF, and the shape parameter $q > 0$. For $q = 1/2$, $q = 1$, and $q = 2$, the GGD represents the Gamma distribution, Laplacian distribution, and Gaussian distribution, respectively. The case of Gaussian distribution will be studied thoroughly in Secs. IV and V. In the following, we mainly focus on the cases of sub-Gaussian ($0 < q < 2$) and sup-Gaussian ($q > 2$) distributions and make a comparative study of the results with that of the Gaussian case.

The TWF after propagation can be formally expressed in terms of the propagator in Eq. (3) acting on the initial representation (5) as

$$\begin{aligned} \psi_L(t) = & \sqrt{\frac{q}{8\pi i\alpha\beta L\Gamma(1/q)}} \exp\left(\frac{it^2}{4\beta L}\right) \\ & \times \int_{-\infty}^{\infty} \exp\left(-\frac{it}{2\beta L}\tau + \frac{i}{4\beta L}\tau^2 - \frac{1+iC}{2\alpha^q}|\tau|^q\right) d\tau. \end{aligned} \quad (6)$$

The relative ratio $\Gamma = \sigma_L/\sigma$ is used to quantify the broadening of generalized Gaussian modes. For the case of Gaussian mode $q = 2$, the ratio Γ can be written in the analytical form as studied in Sec. IV. However, for the general cases of sub- and sup-Gaussian modes, we can obtain it only numerically and follow it versus the transmission distance L .

B. Results and analysis

In this section, we delve into the impact of chromatic dispersion on the broadening of generalized Gaussian modes, characterized by the shape parameter q . The quantification of this impact is achieved through the computation of the broadening parameter Γ .

In this analysis, let us assume the initial SD equals $\sigma = 4.25$ ps. As for the dispersive medium, we compare fiber-based propagation with FSO transmission. We consider $\beta = 20.05 \frac{\text{fs}^2}{\text{m}}$ for the air [33] and $\beta = -1.15 \times 10^{-26} \frac{\text{s}^2}{\text{m}}$ for a typical single-mode optical fiber (SMF).

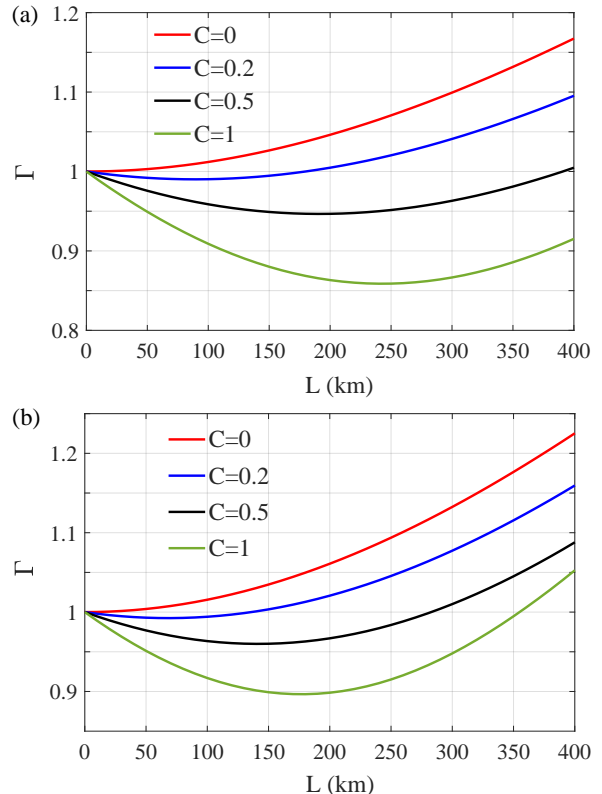


FIG. 1. The broadening parameter, Γ , for $L \in [0, 400]$ km, $\sigma = 4.25$ ps and four values of C for (a) the sub-Gaussian mode $q = 1$ and (b) the sup-Gaussian mode $q = 8$. The transmission through the air is considered, i.e. $\beta = 20.05 \frac{\text{fs}^2}{\text{m}}$.

The observed trends in the broadening parameter for generalized Gaussian modes are intriguing and offer significant insights. Remarkably, for nonzero chirp parameters, the parameter does not exhibit a monotonous behavior with increasing propagation distance. Instead, it follows a pattern, characterized by an initial decrease, reaching a minimum, and subsequently an increase.

In Fig. 1, two distinct cases are considered, namely $q = 1$ (Fig. 1 (a)) and $q = 8$ (Fig. 1 (b)), assuming the transmission through the air. These figures provide valuable insight into how the shape parameter influences the broadening behavior. Notably, for $q = 1$, the broadening parameter experiences a deeper decline compared to

$q = 8$. This suggests that the initial mode shape significantly affects how chromatic dispersion impacts the TWF, with $q = 1$ demonstrating a more pronounced mitigation of broadening.

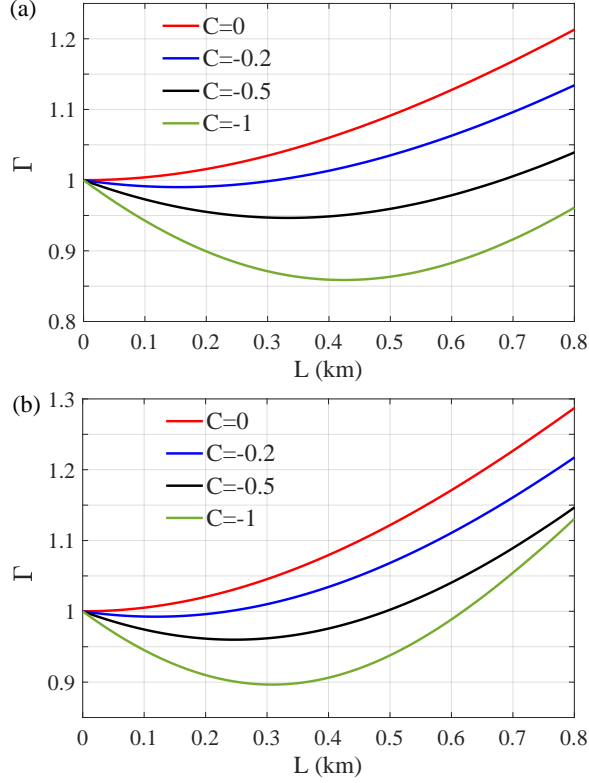


FIG. 2. The broadening parameter, Γ , for $L \in [0, 0.8]$ km, $\sigma = 4.25$ ps and four values of C for (a) the sub-Gaussian mode $q = 1$ and (b) the sup-Gaussian mode $q = 8$. The transmission through an SMF28e+ fiber is considered, i.e. $\beta = -1.15 \times 10^{-26} \frac{\text{fs}^2}{\text{m}}$.

In Fig. 2, a similar scenario is depicted, but the transmission through a typical SMF fiber is considered. To achieve a decline of the broadening parameter, we allow for negative values of the chirp parameter. Due to more significant dispersion, the range of L for which the broadening parameter drops below one is much smaller than in the case of Fig. 1.

In Figs. 1 and 2, within each q , the impact of the chirp parameter is also investigated. The results reveal a direct relationship between the chirp and broadening parameters. Specifically, higher values of $|C|$ are associated with a more profound decline in the broadening parameter. This suggests that effective management of chirp parameters can play a crucial role in mitigating the detrimental effects of chromatic dispersion on generalized Gaussian modes.

Moreover, in Figs. 3 and 4, we present the broadening parameter for various values of q , considering the transmission through the air and an SMF fiber, respectively. The results imply that certain shape parameters may offer superior resistance to chromatic dispersion, allowing

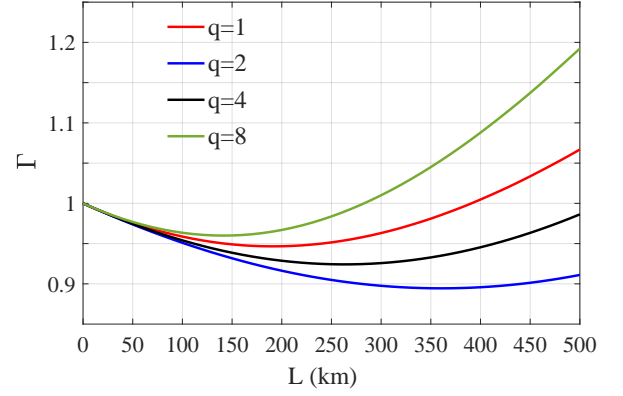


FIG. 3. The broadening parameter, Γ , for $L \in [0, 1.5]$ km, $\sigma = 4.25$ ps, $C = 0.5$ and four values of q . The transmission through the air is considered, i.e. $\beta = 20.05 \frac{\text{fs}^2}{\text{m}}$.

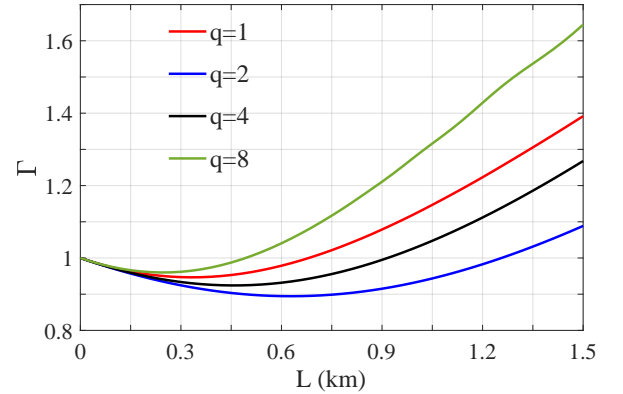


FIG. 4. The broadening parameter, Γ , for $L \in [0, 1.5]$ km, $\sigma = 4.25$ ps, $C = -0.5$ and four values of q . The transmission through an SMF28e+ fiber is considered, i.e. $\beta = -1.15 \times 10^{-26} \frac{\text{fs}^2}{\text{m}}$.

for the maintenance of a narrower TWF over extended propagation distances.

C. Applications in quantum communications

The results on generalized Gaussian modes carry significant implications for the design and implementation of quantum communication systems. Understanding the interplay between shape parameters, chirp values, and chromatic dispersion allows for the optimization of system parameters to achieve high-fidelity transmission over long distances.

In this context, we compute the symbol rate, which is presented in Fig. 5. We consider only fiber-based quantum communication with two values of the chirp parameter: positive ($C = 2$) and negative ($C = -2$).

In the case of positive chirp, presented in Fig. 5 (a), the symbol rate demonstrates a monotonous decrease with increasing propagation distance. This behavior suggests

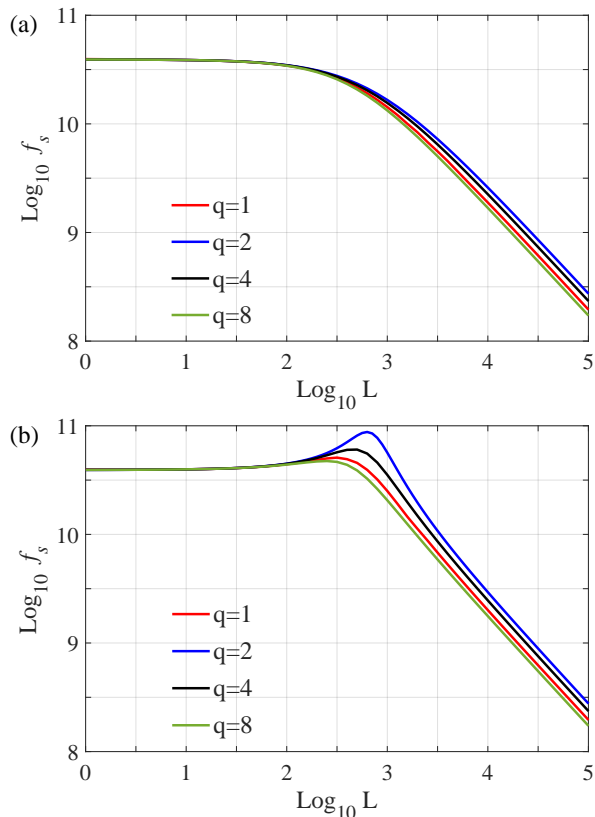


FIG. 5. Symbol rate, f_s , for transmission of photons with generalized Gaussian modes for four values of shape parameter q with (a) positive chirp parameter $C = 2$ and (b) negative chirp parameter $C = -2$ through an SMF28e+ fiber, i.e. $\beta = -1.15 \times 10^{-26} \frac{\text{s}^2}{\text{m}}$. Logarithmic scale is used for L expressed in meters.

a consistent broadening of the temporal mode over the distance, reflecting the challenges posed by chromatic dispersion in maintaining a high symbol rate. Conversely, for the negative chirp, depicted in Fig. 5 (b), the symbol rate exhibits a distinct pattern. Initially, there is an increase in the symbol rate, corresponding to a decline in the temporal width as discussed in the previous section. This transient increase implies a potential advantage in terms of information transfer over short distances. The response of the symbol rate to negative chirp is found to be different for various shape parameters. This observation underscores the sensitivity of quantum communication systems to the intrinsic characteristics of the temporal modes. The variability in the symbol rate's increase suggests that certain shape parameters may allow for more efficient manipulation of chirp-induced effects, leading to improved symbol rates over specific propagation distances.

The research suggests that careful consideration of chirp and shape parameters can be leveraged to optimize symbol rates in quantum communication. The transient increase observed under negative chirp conditions indicates a potential sweet spot for information transfer. Ex-

ploring and exploiting this behavior could pave the way for the development of adaptive quantum communication systems capable of dynamically adjusting to varying propagation conditions.

IV. BROADENING OF CHIRPED GAUSSIAN MODES

A. Methods

Let us consider a temporal mode of a single photon that is Gaussian and can be described by a following TWF

$$\psi(t) = \frac{1}{\sqrt{\sqrt{2\pi}\sqrt{\sigma}}} \exp\left(-\frac{1+iC}{4\sigma^2}t^2\right), \quad (7)$$

where C denotes a chirp parameter, which is related to the squared phase of the temporal mode, cf. [34]. As indicated in Sec. III, this type of TWF is a special case of the generalized Gaussian corresponding to the shape parameter $q = 2$. Nevertheless, chirped Gaussian modes deserve a separate treatment and in-depth analysis due to their significance for laser physics.

By using the propagator given in Eq. (3), we arrive at the formula to describe the TWF after propagation

$$\psi_L(t) = \frac{(1-i) \exp\left(\frac{1+iC}{4(C-i)L\beta-4\sigma^2}t^2\right)}{2^{3/4} \pi^{1/4} \sqrt{\frac{L\beta(1+iC)-i\sigma^2}{\sigma}}} \text{ for } \beta > 0 \quad (8)$$

and

$$\psi_L(t) = \frac{(-2\pi)^{-1/4} \exp\left(\frac{1+iC}{4(C-i)L\beta-4\sigma^2}t^2\right)}{\sqrt{\frac{i[(i-C)L\beta+\sigma^2]}{\sigma}}} \text{ for } \beta < 0. \quad (9)$$

Then, we compute the SD of the modified PDF function. We obtain

$$\sigma_L = \frac{\sqrt{L^2\beta^2 + (\sigma^2 - CL\beta)^2}}{\sigma}, \quad (10)$$

for both $\beta > 0$ and $\beta < 0$.

Finally, we get the relative ratio σ_L/σ to quantify the broadening of chirped Gaussian modes

$$\begin{aligned} \Gamma &= \frac{\sqrt{L^2\beta^2 + (\sigma^2 - CL\beta)^2}}{\sigma^2} \\ &= \sqrt{\left(1 - \frac{CL\beta}{\sigma^2}\right)^2 + \left(\frac{L\beta}{\sigma^2}\right)^2}. \end{aligned} \quad (11)$$

B. Results and analysis

We notice that when $\beta > 0$, we obtain an initial decrease in the photon's width for every $C > 0$. This

tendency is depicted in Fig. 6, where the transmission through the air is considered for selected values of the chirp parameter. The initial width parameter was the same as in Sec. III, i.e. $\sigma = 4.25$ ps.

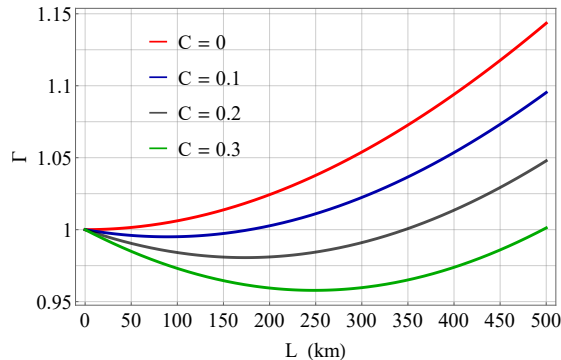


FIG. 6. The broadening parameter, Γ , for $L \in [0, 500]$ km and four values of C . The transmission through the air is considered, i.e. $\beta = 20.05 \frac{\text{fs}^2}{\text{m}}$.

One can observe that the higher the value of C , the more significant decline in the width we obtain. To quantify this phenomenon, we solve

$$\frac{d\Gamma}{dL} = 0,$$

which leads to

$$L_{min} = \frac{C\sigma^2}{(1+C^2)\beta}. \quad (12)$$

The formula (12) provides the transmission distance that corresponds to the minimal value of the temporal width, which is

$$\sigma_L^{min} = \frac{\sigma}{\sqrt{1+C^2}}. \quad (13)$$

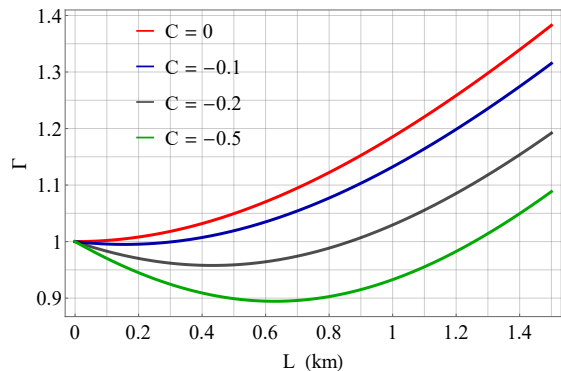


FIG. 7. The broadening parameter, Γ , for $L \in [0, 1.5]$ km and four values of C . The transmission through an SMF28e+ fiber is considered, i.e. $\beta = -1.15 \times 10^{-26} \frac{\text{s}^2}{\text{m}}$.

For $C = 0.3$, we obtain $L_{min} \approx 250$ km, which corresponds to $\Gamma \approx 0.958$. Moreover, when $L = 500$ km,

then $\Gamma \approx 1$, which means that the pulse regains its initial width.

Furthermore, dispersion in an SMF28e+ fiber can be investigated, for which $\beta = -1.15 \times 10^{-26} \frac{\text{s}^2}{\text{m}}$. In such a case, negative chirp parameters have to be incorporated to witness a decrease in the temporal width. In Fig. 7, the results are presented. One can immediately notice that the overall impact of dispersion on the temporal shape of photons is much more significant than in the case of Fig. 6. Nevertheless, up to some distance, one can still control the broadening by adjusting the chirp parameter so that the pulse spreading is not substantial.

C. Applications in quantum communications

The results presented in Sec. IV B focused on the fact that for chirped Gaussian TWF, one can modulate the phase C so that the broadening parameter initially declines toward its minimum value. Now, let us analyze what happens if we consider long-distance quantum communications. In this context, we again use the concept of symbol rate given by

$$f_S = \left(6 \frac{\sqrt{L^2\beta^2 + (\sigma^2 - CL\beta)^2}}{\sigma} \right)^{-1}. \quad (14)$$

In the logarithmic scale, we compute f_S up to $L = 10000$ km, which may correspond to the length of inter-continental fiber-based links. We consider two scenarios – the positive (in Fig. 8) and the negative (in Fig. 9) values of the chirp parameter.

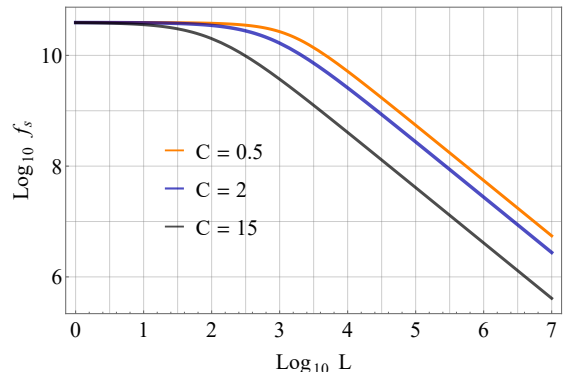


FIG. 8. Symbol rate, f_S , for transmission of photons with Gaussian modes with positive chirp parameters through an SMF28e+ fiber, i.e. $\beta = -1.15 \times 10^{-26} \frac{\text{s}^2}{\text{m}}$. Logarithmic scale is used for L expressed in meters.

From Fig. 8, when $C\beta < 0$, it can be seen that the decreasing trend of the symbol rate depends not only on the increase of the transmission distance L but also on the values of the chirp parameter C . As expected, for short transmission lengths (up to $L \approx 10$ m), the effect of the chirp parameter on f_S is insignificant. However,

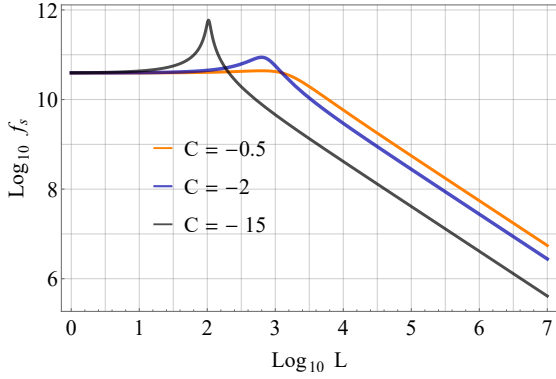


FIG. 9. Symbol rate, f_S , for transmission of photons with Gaussian modes with negative chirp parameters through an SMF28e+ fiber, i.e. $\beta = -1.15 \times 10^{-26} \frac{\text{s}^2}{\text{m}}$. Logarithmic scale is used for L expressed in meters.

the symbol rate decreases more rapidly for higher values of C over long transmission distances.

For a comparative study between the effects of positive and negative chirp parameters on f_S , we draw Fig. 9 for $C\beta > 0$. The general behavior of the curves in Fig. 9 is the same as Fig. 8 for large values of L . However, for $L \lesssim 1$ km, we find that the symbol rate boosts but experiences a sudden decline afterwards. As $|C|$ increases, the downward tendency of f_S is more significant. At the same time, for the greatest absolute value of the chirp parameter, i.e. $|C| = 15$, we observe the most meaningful boost in the symbol rate, but it lasts only up to $L = 100$ m.

Therefore, the negative values of the chirp parameter in short transmission distances have a different effect on the symbol rate, which causes a significant change in the shape and invalidates the monotonic behavior of the curves compared to Fig. 8. Note that the curves of the function f_S in Fig. 9 decline more sharply than those in Fig. 8 for greater $|C|$.

For a deeper understanding of the effects of the chirp parameter and transmission distance on the symbol rate, we rewrite expression Eq. (14) when C and L tend to infinity, namely

$$f_S(C) |_{C \rightarrow \pm\infty} \approx \frac{\sigma}{6C\sqrt{L^2\beta^2}} + \frac{\sigma^3\sqrt{L^2\beta^2}}{6C^2(L\beta)^3} - \frac{\sqrt{L^2\beta^2}(L^2\beta^2\sigma - 2\sigma^5)}{12C^3(L\beta)^4} \quad (15)$$

and

$$f_S(L) |_{L \rightarrow \infty} \approx \frac{\sigma}{6L\sqrt{\beta^2(C^2+1)}} + \frac{\beta C\sigma^3}{6L^2[\beta^2(C^2+1)]^{3/2}} + \frac{\beta^2(2C^2-1)\sigma^5}{12L^3[\beta^2(C^2+1)]^{5/2}}. \quad (16)$$

According to Eqs. (15) and (16), we find that L is a dominant parameter in reducing the symbol rate, and

the large values of the chirp parameter (both positive and negative) have destructive effects on it at large distances. These results are in good agreement with Figs. 8 and 9.

V. GAUSSIAN MODE BROADENING

A. Methods

As a special case, let us consider a plain Gaussian mode deprived of a relative phase. In such a case, we assume that the temporal mode of a single photon can be described by a function as

$$\psi(t) = \frac{1}{\sqrt{\sqrt{2\pi}\sqrt{\sigma}}} \exp\left(-\frac{t^2}{4\sigma^2}\right), \quad (17)$$

where σ represents the initial width of the pulse, i.e. the SD of the Gaussian distribution related to the wave packet.

The action of the propagator (3) provides the following results

$$\psi_L(t) = \frac{(1-i)\exp\left(-\frac{t^2}{4iL\beta+4\sigma^2}\right)}{2^{3/4}\pi^{1/4}\sqrt{\frac{L\beta}{\sigma}-i\sigma}} \quad \text{for } \beta > 0 \quad (18)$$

and

$$\psi_L(t) = \frac{(-2\pi)^{-1/4}\exp\left(-\frac{t^2}{4iL\beta+4\sigma^2}\right)}{\sqrt{-\frac{L\beta}{\sigma}+i\sigma}} \quad \text{for } \beta < 0. \quad (19)$$

The formulas (18) and (19) represent the TWF after propagation through a medium that features normal and anomalous dispersion regimes, respectively.

When we compute the SD of the PDF after propagation, we obtain one result irrespective of the dispersion regime

$$\sigma_L = \frac{\sqrt{L^2\beta^2 + \sigma^4}}{\sigma}. \quad (20)$$

Finally, the relative ratio σ_L/σ to quantify the broadening can be obtained as

$$\Gamma = \frac{\sqrt{L^2\beta^2 + \sigma^4}}{\sigma^2} = \sqrt{1 + \frac{L^2\beta^2}{\sigma^4}}, \quad (21)$$

which agrees with Eq. (11) for $C = 0$. This result allows us to study how the temporal shape of a single photon changes as a consequence of chromatic dispersion.

B. Results and analysis

When a photon with a plain Gaussian mode Eq. (17) is transmitted through a dispersive medium, it broadens in the time domain. The degree of broadening can be

quantified by the relative ratio given by Eq. (21). Γ can be treated as a function of L , which is the independent variable. Moreover, the broadening ratio Γ depends on the GVD parameter. According to Eq. (21), for higher values of β , the degree of broadening is more significant (for both positive and negative GVD parameters).

TABLE I. GVD parameters based on Ref. [33].

| Nitrogen | Air | Oxygen | Carbon Dioxide |
|--------------------------------------|--------------------------------------|--------------------------------------|--------------------------------------|
| $18.70 \frac{\text{fs}^2}{\text{m}}$ | $20.05 \frac{\text{fs}^2}{\text{m}}$ | $24.76 \frac{\text{fs}^2}{\text{m}}$ | $30.90 \frac{\text{fs}^2}{\text{m}}$ |

Moreover, from Ref. [33], we incorporate four values of the second-order dispersion parameter that correspond to selected gases; see Table I. The dispersion measurements were performed using an ultrabroadband femtosecond oscillator. These data allow for a comparison of different gases in terms of their efficiency in FSO communications.

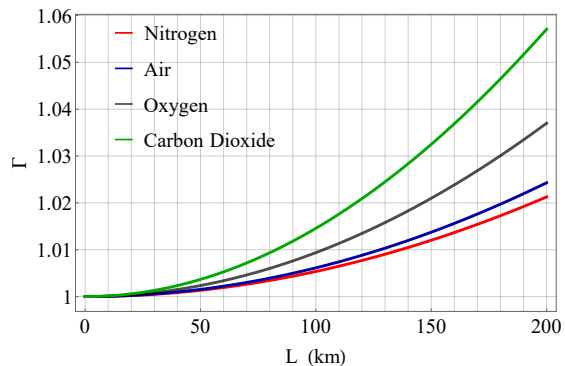


FIG. 10. The broadening parameter, Γ , for $L \in [0, 200]$ km.

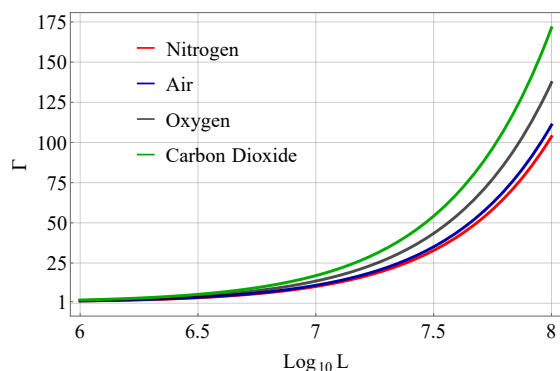


FIG. 11. The broadening parameter, Γ , for $L \in [10^6, 10^8]$ m. A logarithmic scale was used on the horizontal axis.

In Fig. 10, the broadening parameter, Γ , is plotted versus the transmission distance, L . In the case of transmitting a signal through the air, we see that the broadening is not significant for moderate values of L . When $L = 200$

km, the final pulse is approx. 2.5% wider than the initial one. The effects of chromatic dispersion are more substantial if we increase the transmission distance. In Fig. 11, we present Γ versus L in the logarithmic scale.

To conclude, we notice that for short and moderate values of the transmission distance, the broadening is not significant for the selected gases. However, the broadening increases with L , meaning that at a longer propagation distance, the broadening is more critical, which can be observed more clearly on a logarithmic scale. By following this method, one can compute Γ according to Eq. (21) to precisely evaluate the impact of chromatic dispersion under any circumstances (for a specific transmission distance and GVD parameter).

C. Applications in quantum communications

For Gaussian wave packets, we experience only broadening irrespective of the sign of β . The fact that the photon's temporal mode is stretched negatively affects the symbol rate in quantum communications. For Gaussian modes, the symbol rate reads

$$f_s = \left(6 \sqrt{\left(\frac{L\beta}{\sigma} \right)^2 + \sigma^2} \right)^{-1}. \quad (22)$$

In Fig. 12, we present the results, where the logarithmic scale has been used for better clarity. We consider two values of the GVD parameter – one corresponding to the air (given in Table I) and the other related to a typical SMF, i.e. $\beta = -1.15 \times 10^{-26} \frac{\text{s}^2}{\text{m}}$. From Fig. 12, we see that initially, the symbol rate approximates $f_s \approx 40$ GBd. At some points, both plots start to decline, but for the air the drop-off occurs later and the curve is above the fiber.

The above analysis can determine how beneficial it is to establish an FSO channel and perform quantum communications. While FSO techniques may allow a higher

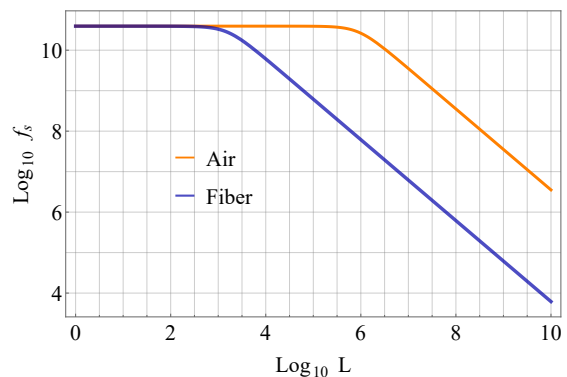


FIG. 12. Symbol rate, f_s , for transmission of single photons with Gaussian modes in a fiber and through the air. The logarithmic scale is used for L expressed in meters.

symbol rate, one should bear in mind the significant limitations of such links, for example, pointing errors and turbulence-induced fluctuations. Furthermore, since we do not take into account any photon loss, the results can be treated as a theoretical limit, namely an upper bound for the symbol rate.

VI. EFFECTS OF CHROMATIC DISPERSION ON TIME-BIN ENCODED QUBITS

A. Qubit encoded in the time domain

Time-bin qubit can be defined as a photon delocalized in the time domain in two wave packets separated by an interval T [31]. Such a state can be produced by using a Mach-Zehnder interferometer to introduce a difference in the optical path. In addition, let us assume that both wave packets are Gaussian and gain an initial chirp parameter, which leads to a time-bin qubit in the form

$$\psi(t) = a \varphi\left(t - \frac{T}{2}\right) + b \varphi\left(t + \frac{T}{2}\right), \quad (23)$$

where

$$\varphi(t) = \frac{1}{\sqrt{\sqrt{\pi}\sqrt{\sigma}}} \exp\left(-\frac{1+iC}{2\tilde{\sigma}^2} t^2\right). \quad (24)$$

The coefficients a and b from Eq. (23) satisfy

$$|a|^2 + |b|^2 = 1, \quad (25)$$

which means that one can substitute $a = \cos(\theta/2)$ and $b = \sin(\theta/2)e^{i\phi}$, where $\theta \in [0, \pi]$ and $\phi \in [0, 2\pi)$. In addition, One can notice that the symbol $\tilde{\sigma}$ relates to the width of one wave packet.

For the wave function (23), we define the PDF in a standard way $p(t) := \psi^*(t)\psi(t)$. One can compute

$$\int_{-\infty}^{\infty} p(t) dt = 1 + \sin\theta \cos\phi \exp\left(-\frac{1+C^2}{4\tilde{\sigma}^2} T^2\right). \quad (26)$$

The result in Eq. (26) indicates that there is a non-zero overlap between the basis functions. However, the PDF can be roughly normalized by adjusting the ratio $T^2/\tilde{\sigma}^2$. Since T can be easily controlled in the laboratory by regulating the length of the optical path, one can ensure that for well-separated pulses and a given chirp parameter, we have $\exp\left\{-\frac{(1+C^2)T^2}{4\tilde{\sigma}^2}\right\} \approx 0$. Fig. 13 presents the PDF for a qubit composed of two well-separated wave packets.

After propagation through a dispersive medium, the qubit is represented as

$$\psi_L(t) = a \varphi_L\left(t - \frac{T}{2}\right) + b \varphi_L\left(t + \frac{T}{2}\right), \quad (27)$$

where $\varphi_L(t) := \int_{-\infty}^{\infty} \mathcal{S}(t, \tau, L) \varphi(\tau) d\tau$. Fig. 14 shows, for specific values of the parameters, six PDFs after propagation defined as $p_L(t) := \psi_L^*(t)\psi_L(t)$. We take into

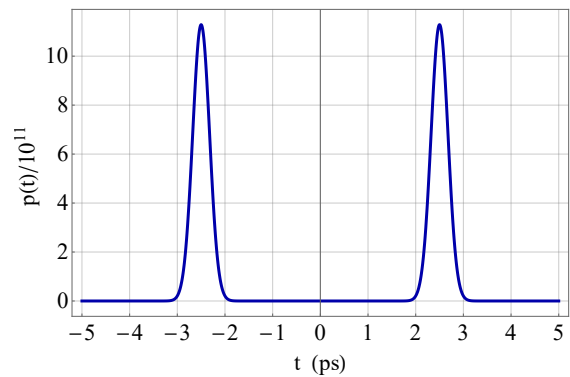


FIG. 13. The PDF, $p(t)$, for a time-bin qubit before propagation through a dispersive medium. The parameters were: $T = 5$ ps, $\tilde{\sigma} = 0.25$ ps, $C = 2$, $\theta = \pi/2$, and $\phi = \pi/4$.

account three fiber lengths L and two values of the phase C (zero and non-zero) to demonstrate how both quantities affect the temporal mode of the qubit.

From the top panel of Fig. 14, when C is zero, one can see how the PDF, $p_L(t)$, for a time-bin qubit after propagation through a dispersive medium changes as we increase L . Indeed, with the increase of L from 100m to 500m, the amplitude of $p_L(t)$ decreases, but it is more stretched over time. In comparison, when we take a non-zero C , the number of fringes increases, as seen from the bottom panel of Fig. 14. Therefore, the non-zero chirp parameter has a significant effect on $p_L(t)$ since it affects it twofold – by changing the number of fringes and increasing the temporal length of the qubit.

B. Results and analysis

Due to the mathematical complexity of Eq. (27), it is not possible to compute analytically the variance of the $p_L(t)$. Therefore, we proceed to this task numerically by discretization of the independent variable L . For fixed values of all parameters and variables, we obtain explicit one-variable functions: $p(t)$ and $p_L(t)$, for which we can compute the corresponding SDs, i.e. σ , σ_L , and then the broadening parameter as $\Gamma = \sigma_L/\sigma$. By changing L step by step, we generate dotted plots that present the properties of the broadening parameter Γ .

Fig. 15 shows the results for the propagation through the air while Fig. 16 includes the findings for a standard fiber. In both cases, all the parameters characterizing the qubit were fixed, i.e. $T = 5$ ps, $\tilde{\sigma} = 0.25$ ps, $\theta = \pi/2$, and $\phi = 0$ (the same as in Fig. 14).

In Fig. 15, we plot the broadening parameter Γ versus propagation length L for four values of C when the transmission through the air is considered. We witness that Γ is linear and the angle grows as the value of the chirp parameter increases from 0 to 3. By comparing Figs. 6 and 15, it can be seen that the effects of the chirp parameter on the broadening of two wave packets after propaga-

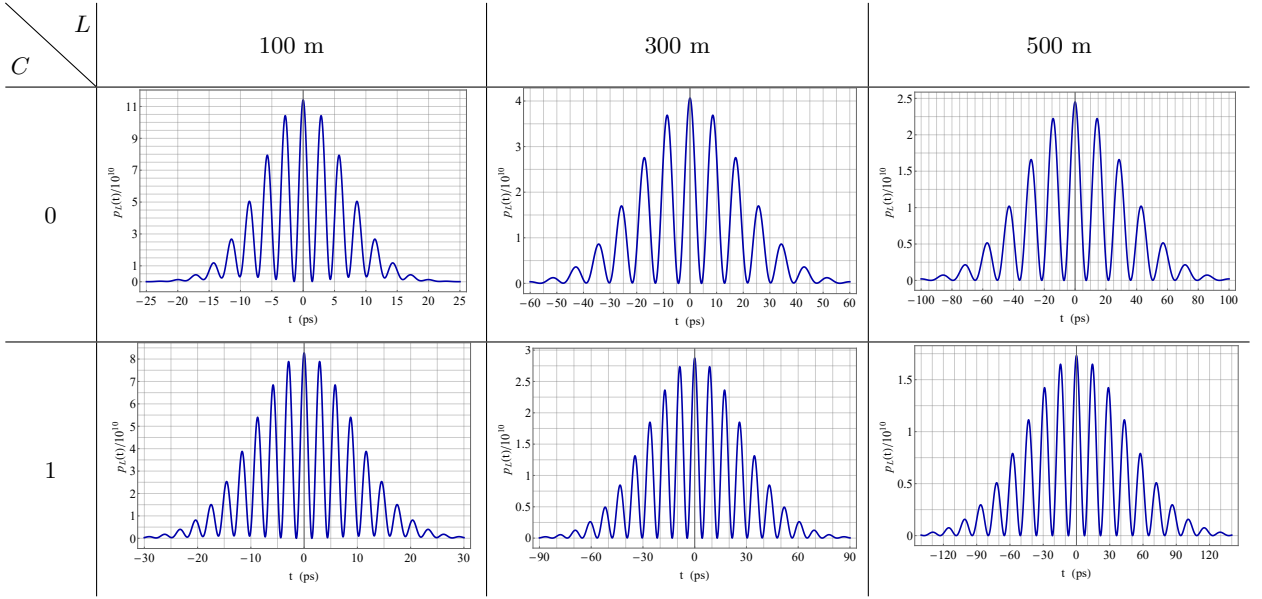


FIG. 14. Six PDFs, $p_L(t)$, for a time-bin qubit after propagation through a dispersive medium, for different fiber lengths L and phases C . The parameters were: $\beta = -1.15 \times 10^{-26} \frac{\text{s}^2}{\text{m}}$, $T = 5$ ps, $\tilde{\sigma} = 0.25$ ps, $\theta = \pi/2$, and $\phi = 0$.

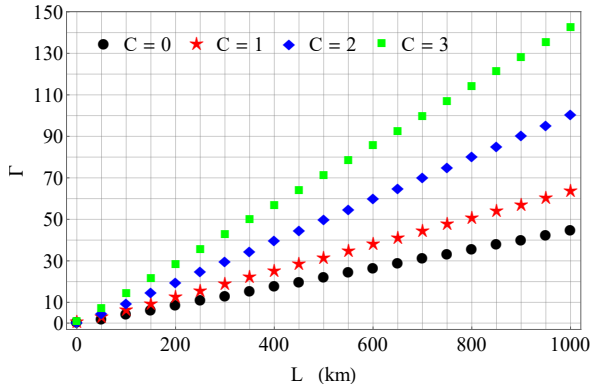


FIG. 15. Qubit's broadening parameter, Γ , for $L \in [0, 1000]$ km and four values of C . The transmission through the air is considered, i.e. $\beta = 20.05 \frac{\text{fs}^2}{\text{m}}$.

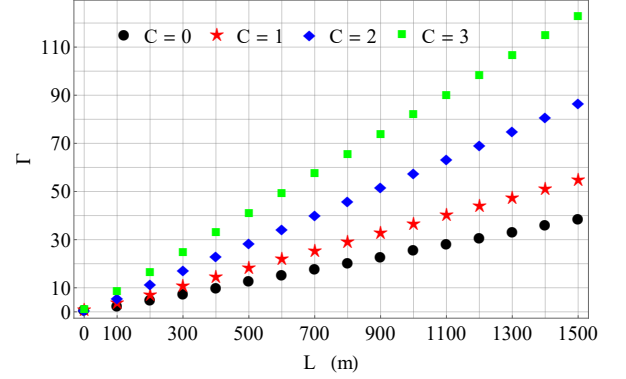


FIG. 16. Qubit's broadening parameter, Γ , for $L \in [0, 1500]$ m and four values of C . The transmission through an SMF28e+ fiber is considered, i.e. $\beta = -1.15 \times 10^{-26} \frac{\text{s}^2}{\text{m}}$.

tion given by Eqs. (8) and (27) are completely different. In addition, the value of qubit's broadening in Fig. 15 is significant for long transmission lengths compared to Fig. 6.

When $C\beta \leq 0$, we illustrate the qubit's broadening as a function of L during the transmission through an SMF28e+ fiber in Fig. 16. The qualitative behavior of Γ for distinct values of the chirp parameter in this figure is similar to Fig. 15, but the quantitative behavior is different due to more significant dispersion in the fiber than in the air. Hence, the value of Γ can be remarkably controlled by adjusting the chirp parameter to the transmission medium.

VII. BROADENING OF HYPERBOLIC-SECANT MODES

A. Methods

Let us consider a temporal mode of a single photon that is hyperbolic-secant and can be expressed by a TWF as

$$\psi(t) = \sqrt{\frac{1}{2\sigma} \text{Sech} \frac{\pi t}{2\sigma}} \exp\left(-\frac{iCt^2}{4\sigma^2}\right). \quad (28)$$

The wave function changes due to dispersion in terms of the propagator (3) acting on the initial TWF (28). It

can be expressed as

$$\psi_L(t) = \frac{\exp\left(\frac{it^2}{4\beta L}\right)}{\sqrt{8\pi i\beta L\sigma}} \int_{-\infty}^{\infty} \sqrt{\frac{2}{e^{\pi\tau/(2\sigma)} + e^{-\pi\tau/(2\sigma)}}} \times \exp\left\{-i\left(\frac{t}{2\beta L}\tau + \left(\frac{1}{4\beta L} - \frac{C}{4\sigma^2}\right)\tau^2\right)\right\} d\tau. \quad (29)$$

The broadening parameter Γ of the hyperbolic-secant modes cannot be computed analytically. Similarly to the cases of generalized Gaussian modes, we can obtain Γ numerically for the specific parameters characterizing hyperbolic-secant modes.

B. Results and analysis

The results presented in this section focus on the chirp parameter as a crucial factor. We also distinguish two scenarios – positive and negative dispersions.

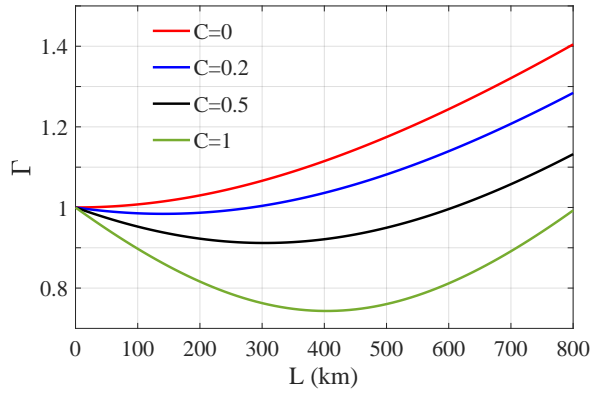


FIG. 17. The broadening parameter, Γ , for $L \in [0, 800]$ km, $\sigma = 4.25$ ps and four non-negative values of C for the hyperbolic-secant pulses. The transmission through the air is considered, i.e. $\beta = 20.05 \frac{\text{fs}^2}{\text{m}}$.

In Fig. 17, we present the plots for positive dispersion and non-negative chirp parameters. The dependence of the broadening parameter on the chirp parameter suggests that careful adjustment of the chirp can effectively mitigate the detrimental effects of normal dispersion. The presence of a minimum in broadening indicates an optimal chirp value for minimizing temporal spreading. The deeper minimum for higher chirp values suggests a potential optimization strategy. By increasing the chirp, one can achieve a more pronounced reduction in broadening before the subsequent increase. This insight is valuable for practical implementations, allowing for more efficient compensation of dispersion effects.

The monotonic increase in broadening for non-positive chirps highlights a contrasting behavior, as presented in Fig. 18. This could indicate the challenges associated

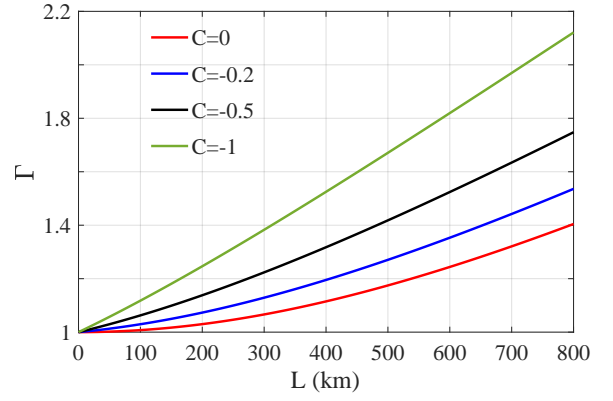


FIG. 18. The broadening parameter, Γ , for $L \in [0, 800]$ km, $\sigma = 4.25$ ps and four non-positive values of C for the hyperbolic-secant pulses. The transmission through the air is considered, i.e. $\beta = 20.05 \frac{\text{fs}^2}{\text{m}}$.

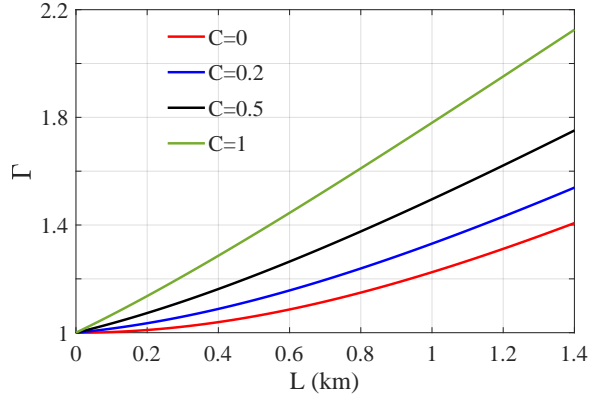


FIG. 19. The broadening parameter, Γ , for $L \in [0, 1.4]$ km, $\sigma = 4.25$ ps and four non-negative values of C for the hyperbolic-secant pulses. The transmission through an SMF28e+ fiber is considered, i.e. $\beta = -1.15 \times 10^{-26} \frac{\text{s}^2}{\text{m}}$.

with compensating for dispersion using certain chirp values, emphasizing the importance of positive chirps for effective dispersion management in FSO communications.

The reversal of trends for negative dispersion is a noteworthy observation. For non-negative chirp parameters, we observe a monotonic increase of Γ , which is provided in Fig. 19 for the transmission through an SMF28e+ fiber. The initial decline in broadening for negative chirps, as given in Fig. 20, suggests a compensatory effect, where selected chirp values counteract the broadening caused by negative dispersion. Tailoring the chirp parameter in the presence of negative dispersion can potentially enhance communication rates over specific distances, offering a novel avenue for system optimization.

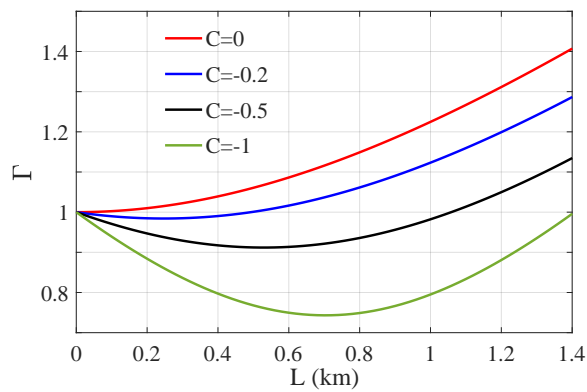


FIG. 20. The broadening parameter, Γ , for $L \in [0, 1.4]$ km, $\sigma = 4.25$ ps and four non-positive values of C for the hyperbolic-secant pulses. The transmission through an SMF28e+ fiber is considered, i.e. $\beta = -1.15 \times 10^{-26} \frac{\text{s}^2}{\text{m}}$.

C. Applications in quantum communications

To investigate the efficiency of hyperbolic-secant modes in fiber-based quantum communications, we compute the symbol rate for negative dispersion, as shown in Fig. 21. The consistent decline in symbol rate with positive chirps underlines the challenging nature of maintaining high communication rates in the presence of anomalous dispersion. These findings emphasize the need for compensatory techniques to counteract the adverse effects of dispersion on communication efficiency.

The observed pitch in the symbol rate for negative chirps introduces a valuable contribution. The ability to tailor the chirp parameter to exploit dispersion for increased communication rates over specific distances presents a strategic advantage. This result opens up possibilities for optimizing quantum communication systems in scenarios involving negative dispersion.

VIII. DISCUSSION AND OUTLOOK

In this paper, we studied the effects of chromatic dispersion on single-photon TWFs. Instead of analyzing classical beams, we operated in the quantum regime and considered wave functions describing the temporal shape of photons. We first analyzed generalized Gaussian modes, which has laid the foundation for more specific representation. As a result, we considered chirped and unchirped Gaussian modes. For chirped modes, we have found out that the chirp parameter allows us to control the broadening of the pulses due to chromatic dispersion. By adjusting the chirp parameter, we were able to mitigate the effects of chromatic dispersion and even prevent the photon shape from being stretched at all. In the case of plain Gaussian modes, when the temporal width broadens irrespective of the type of dispersion, we compared the degree of broadening in different

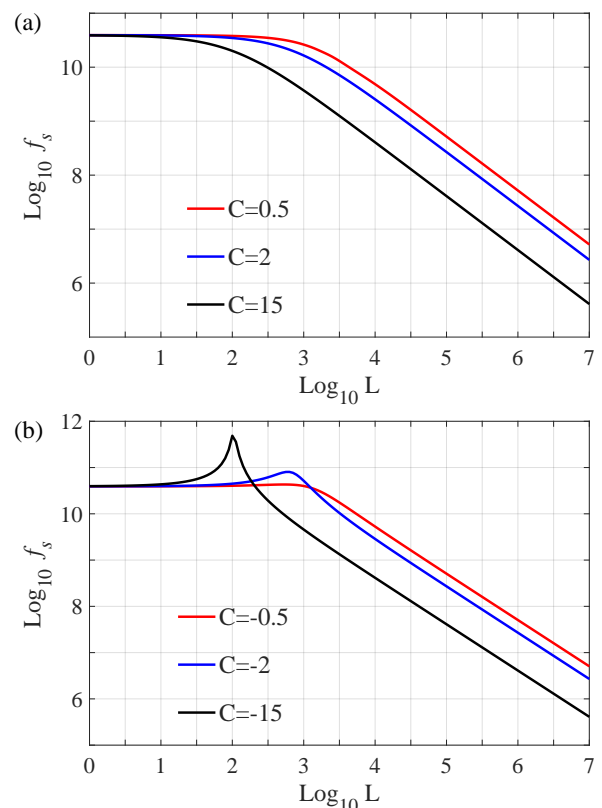


FIG. 21. Symbol rate, f_s , for transmission of photons with hyperbolic-secant pulses with (a) positive chirp parameters and (b) negative chirp parameters through an SMF28e+ fiber, i.e. $\beta = -1.15 \times 10^{-26} \frac{\text{s}^2}{\text{m}}$. Logarithmic scale is used for L expressed in meters.

media. Moreover, we studied the efficiency of quantum communication, showing an advantage of free-space optics techniques as far as the symbol rate is considered.

In addition, we also analyzed the impact of chromatic dispersion on a qubit defined in the temporal degree of freedom. We found that the chirp parameter has a significant impact on the interference pattern of the qubit.

Finally, to go beyond Gaussian-shaped modes, we performed a comprehensive analysis of hyperbolic-secant modes under different dispersion conditions and chirp parameters. These findings provide a robust foundation for advancing the understanding of quantum communication systems.

Overall, our results demonstrate that the chirp parameter is a powerful tool for controlling the effects of chromatic dispersion on temporal modes of single photons. The insights gained from this study offer practical guidelines for system designers, indicating potential strategies for optimizing communication rates and mitigating the effects of chromatic dispersion.

In future research, it would be interesting to study the effects of chromatic dispersion on other types of quantum states, such as entangled photons, and to investigate the use of chirped pulses for quantum communication and

quantum computing applications. Additionally, it would also be interesting to study the impact of other types of dispersion, such as group velocity dispersion, on temporal modes of single photons, and how they could be mitigated using chirped pulses.

In conclusion, our study provides a deeper understanding of the effects of chromatic dispersion on temporal modes of single photons and how it can be mitigated using chirped pulses. Such investigation holds significance in the context of advancing quantum information processing and communication technologies. Thus, the results presented in this paper open up new possibilities for the use of chirped pulses in quantum optics and quantum information processing.

ACKNOWLEDGEMENTS

A.C. acknowledges financial support from the Foundation for Polish Science within the “Quantum Optical Technologies” project carried out within the Interna-

tional Research Agendas programme co-financed by the European Union under the European Regional Development Fund (MAB/2018/4). X.C. acknowledges support from the National Natural Science Foundation of China (Grant No. 12005121). S.H. was supported by Semnan University under Contract No. 21270.

DISCLOSURES

The authors declare that they have no known competing financial interests.

DATA AVAILABILITY

No datasets were generated or analyzed during the current study.

-
- [1] N. Gisin and R. Thew, Quantum communication. *Nature Photon.* **1**, 165–171 (2007).
- [2] G. Cariolaro, *Quantum Communications. Signals and Communication Technology* (Springer Cham, Heidelberg 2015).
- [3] R. Renner, Security of quantum key distribution. *Int. J. Quantum Inf.* **6**, 1–127 (2008).
- [4] V. Scarani, H. Bechmann-Pasquinucci, N. J. Cerf, M. Dusek, N. Lutkenhaus, and M. Peev, The security of practical quantum key distribution. *Rev. Mod. Phys.* **81**, 1301 (2009).
- [5] C. Portmann and R. Renner, Security in quantum cryptography. *Rev. Mod. Phys.* **94**, 025008 (2022).
- [6] E. Hecht, *Optics. Global edition* (Pearson Education Limited, Harlow 2017).
- [7] S. L. Braunstein and P. van Loock, Quantum information with continuous variables. *Rev. Mod. Phys.* **77**, 513 (2005).
- [8] X.-B. Wang, T. Hiroshima, A. Tomita, and M. Hayashi, Quantum information with Gaussian states. *Phys. Rep.* **448**, 1–111 (2007).
- [9] C. Weedbrook, S. Pirandola, R. Garcia-Patron, N. J. Cerf, T. C. Ralph, J. H. Shapiro, and S. Lloyd, Gaussian quantum information. *Rev. Mod. Phys.* **84**, 621 (2012).
- [10] C. Weedbrook, Continuous-variable quantum key distribution with entanglement in the middle. *Phys. Rev. A* **87**, 022308 (2013).
- [11] P. Jouguet, S. Kunz-Jacques, A. Leverrier, P. Grangier, and E. Diamanti, Experimental demonstration of long-distance continuous-variable quantum key distribution. *Nature Photon.* **7**, 378–381 (2013).
- [12] T. C. Zhang, K. W. Goh, C. W. Chou, P. Lodahl, and H. J. Kimble, Quantum teleportation of light beams. *Phys. Rev. A* **67**, 033802 (2003).
- [13] H. S. Qureshi, S. Ullah, and F. Ghafoor, Continuous variable quantum teleportation via entangled Gaussian state generated by a linear beam splitter. *J. Phys. B: At. Mol. Opt. Phys.* **53**, 135501 (2020).
- [14] J. D. Franson, Bell inequality for position and time. *Phys. Rev. Lett.* **62**, 2205 (1989).
- [15] I. Marcikic, H. de Riedmatten, W. Tittel, V. Scarani, H. Zbinden, and N. Gisin, Time-bin entangled qubits for quantum communication created by femtosecond pulses. *Phys. Rev. A* **66**, 062308 (2002).
- [16] J. M. Donohue, M. Agnew, J. Lavoie, and K. J. Resch, Coherent ultrafast measurement of time-bin encoded photons. *Phys. Rev. Lett.* **111**, 153602 (2013).
- [17] T. Pittman, It’s a good time for time-bin qubits. *Physics* **6**, 110 (2013).
- [18] J. Brendel, N. Gisin, W. Tittel, and H. Zbinden, Pulsed Energy-Time Entangled Twin-Photon Source for Quantum Communication, *Phys. Rev. Lett.* **82**, 2594 (1999).
- [19] A. Czerwinski and J. Szlachetka, Efficiency of photonic state tomography affected by fiber attenuation. *Phys. Rev. A* **105**, 062437 (2022).
- [20] S. H. Wemple, Material dispersion in optical fibers. *Appl. Opt.* **18**, 31 (1979).
- [21] M. Miyagi and S. Nishida, Pulse spreading in a single-mode optical fiber due to third-order dispersion: effect of optical source bandwidth. *Appl. Opt.* **18**, 2237–2240 (1979).
- [22] D. Marcuse, Pulse distortion in single-mode fibers. *Appl. Opt.* **19**, 1653–1660 (1980).
- [23] K. Iwashita and N. Takachio, Chromatic dispersion compensation in coherent optical communications. *J. Light. Technol.* **8**, 367–375 (1990).
- [24] M. Malekiha, I. Tselniker, and D. V. Plant, Chromatic dispersion mitigation in long-haul fiber-optic communication networks by sub-band partitioning. *Opt. Express*

- 23**, 32654–32663 (2015).
- [25] F. Rottenberg, T.H. Nguyen, S.P. Gorza, F. Horlin, and J. Louveaux, Advanced chromatic dispersion compensation in optical fiber FBMC-OQAM systems. *IEEE Photonics J.* **9**, 1–10 (2017).
- [26] M. Lasota and P. Kolenderski, Quantum communication improved by spectral entanglement and supplementary chromatic dispersion. *Phys. Rev. A* **98**, 062310 (2018).
- [27] C. G. B. Garrett and D. E. McCumber, Propagation of a Gaussian Light Pulse through an Anomalous Dispersion Medium. *Phys. Rev. A* **1**, 305 (1970).
- [28] G. P. Agrawal, *Nonlinear fiber optics (Fifth Edition)*, (Academic Press, Oxford 2013)
- [29] M. G. Raymer and I. A. Walmsley, Temporal modes in quantum optics: then and now. *Phys. Scr.* **95**, 064002 (2020).
- [30] K. Sedziak, M. Lasota, and P. Kolenderski, Reducing detection noise of a photon pair in a dispersive medium by controlling its spectral entanglement. *Optica* **4**, 84–89 (2017).
- [31] K. Sedziak-Kacprowicz, A. Czerwinski, and P. Kolenderski, Tomography of time-bin quantum states using time-resolved detection. *Phys. Rev. A* **102**, 052420 (2020).
- [32] A. Czerwinski, K. Sedziak-Kacprowicz, and P. Kolenderski, Phase estimation of time-bin qudits by time-resolved single-photon counting. *Phys. Rev. A* **103**, 042402 (2021).
- [33] P. J. Wrzesinski, D. Pestov, V. V. Lozovoy, J. R. Gord, M. Dantus, and S. Roy, Group-velocity-dispersion measurements of atmospheric and combustion-related gases using an ultrabroadband-laser source. *Opt. Express* **19**, 5163–5170 (2011).
- [34] D. Marcuse, Pulse distortion in single-mode fibers. 3: Chirped pulses. *Appl. Opt.* **20**, 3573–3579 (1981).